CBPF-NF-033/82

FIRST- AND SECOND-NEIGHBOR SQUARE LATTICE POTTS MODEL: RENORMALIZATION GROUP TREATMENT

by

P. Murilo Oliveira[1]*, C. Tsallis[2]
and G. Schwachheim[2]

[1]INSTITUTO DE FÍSICA
Universidade Federal Fluminense
Caixa Postal 296
Niteroi, RJ - BRAZIL

[2]CENTRO BRASILEIRO DE PESQUISAS FÍSICAS/CNPq
Rua Xavier Sigaud, 150
22290 - Rio de Janeiro, RJ - BRAZIL

*Partially supported by CNPq and FINEP(Brazilian Agencies)

FIRST- AND SECOND-NEIGHBOR SQUARE LATTICE POTTS MODEL: RENORMALIZATION GROUP TREATMENT.

P. Murilo Oliveira*

Instituto de Física
Universidade Federal Fluminense
Caixa Postal 296
Niteroi, RJ - BRAZIL

C. Tsallis and G. Schwachheim

Centro Brasileiro de Pesquisas Físicas/CNPq
Rua Xavier Sigaud, 150
22290 - Rio de Janeiro, RJ - BRAZIL

*Partially supported by CNPq and FINEP(Brazilian Agencies)

ABSTRACT

Within a real space renormalization group framework, we study the q-state Potts model in square lattice assuming positive second-neighbor coupling constant and arbitrary sign for the first-neighbor one. The q-evolution of the full phase diagram as well as the thermal and magnetic critical exponents is obtained. Whenever comparison with available results is possible, the agreement is either exact or very satisfactory.

I - INTRODUCTION

The first- and second-neighbor square lattice is not a strictly planar one, and the q-state Potts model exact phase diagram is not yet available for any finite value of q. In what concerns the critical exponents they are expected to be, for positive second-neighbor coupling constant (i.e. no frustration), the same as for strictly planar lattices, presumably the den Nijs conjecture [1] for the thermal critical exponent y_T and Nienhuis et al conjecture [2] for the magnetic one y_H. The q = 2 case (Ising model) has been treated [3] within a real space renormalization group (RG) framework which provided qualitatively (but not quantitatively) satisfactory results. More recently good numerical estimates have been provided [4] by high temperature series expansion. The q = 1 case (bond percolation) has been treated [5] within a RG formalism; the corresponding critical line recovers in both extremities (only first- or only second-neighbor bonds) the exact results; the numerical estimates for both "thermal" and "magnetic" critical exponents are quite satisfactory. In what concerns the exponent y_H, advantage is therein taken from the fact that, in the limit of vanishing first-neighbor coupling constant, two simple square lattices are decoupled; this fact enables [3,5,6] the calculation of y_H without introducing any external field.

In the present paper we follow along the lines of Ref. [5] and, by using the geometrical formulation of the Potts model as introduced in Ref. [7], we extend, to all values of $q \leq 4$, the discussion of the phase diagram and both y_T and y_H exponents for the first- and second-neighbor square lattice (on-

ly positive second-neighbor coupling constants are under consideration). For $q > 4$ the transition is a first-order one and is out of the scope of the present approach.

II - RENORMALIZATION GROUP

We consider the Hamiltonian

$$\mathcal{H} = -qJ_1 \sum_{nn} \delta_{\sigma i,\sigma j} - qJ_2 \sum_{nnn} \delta_{\sigma i,\sigma j} \qquad (\sigma_i = 1,2,\ldots,q,\forall i) \tag{1}$$

where the summations are over nearest-neighbor and next-nearest-neighbor pairs respectively, and J_1 and $J_2 \geq 0$ are the coupling constants. Let us introduce convenient variables (hereafter referred to as <u>transmissivities</u>[7]) through the following definition:

$$t_i \equiv \frac{1 - e^{-qJ_i/k_BT}}{1 + (q-1)e^{-qJ_i/k_BT}} \qquad (i = 1,2) \tag{2}$$

Remark that the physical variation interval for t_i is $[0,1]$ if $J_i \geq 0$, $\left[-\frac{1}{q-1}, 0\right]$ if $J_i \leq 0$ and $q \geq 1$, and $[-\infty,0] \cup \left[\frac{1}{1-q}, \infty\right]$ if $J_i \leq 0$ and $q < 1$.

The RG recursive relations are established by applying the Break-collapse method[7] on the family of cells indicated in Fig. 1; we obtain

$$t_1' = R_b(t_1,t_2)$$

$$t_2' = Q_b(t_1,t_2) \tag{3}$$

These relations exhibit in the $0 \leq t_2 \leq 1$ physical region the following fixed points (FP): (0,0) (fully stable; paramagnetic FP), (0,1) and (1,0) (semi-stable), (1,1) (fully stable; ferromagnetic FP), $(-\frac{1}{q-1}, 1)$ (fully stable; antiferromagnetic FP), $(\frac{1}{\sqrt{q}+1}, 0)$ (semi-stable; critical FP), $(0, \frac{1}{\sqrt{q}+1})$ (fully unstable; critical FP) and (t_1^*, t_2^*) (semi-stable; critical FP; $t_1^* \leq 0$, $\forall q$; $t_2^* = 0$ if $0 \leq q \leq q^*$ and $t_2^* > 0$ if $q > q^*$; $q^* \simeq 2.386$ for $b = 2$ and $q^* \simeq 2.482$ for $b = 3$). The full $b = 2$ flux diagrams associated with $q = 1,2,3,4$ are presented in Fig. 2 (similar flux diagrams have also been obtained[8] for the honeycomb lattice Ising model). The $(\frac{1}{\sqrt{q}+1}, 0)$ and $(0, \frac{1}{\sqrt{q}+1})$ critical FP (obtained for all values of b) recover the simple square lattice exact result[9]. This is not so for the (t_1^*, t_2^*) critical FP as the exact result[10] corresponds to $t_1^* = (\sqrt{4-q}-2)/(\sqrt{4-q}-2+q)$ and $t_2^* = 0$ for $0 \leq q \leq 3$ (i.e. $q^* = 3$; remark that our values for q^*, respectively 2.386 and 2.482 for $b = 2$ and $b = 3$, present the correct tendency). Furthermore, within the RG formalism, it is natural to expect that, for $q > 3$, $t_1^* = -\frac{1}{q-1}$ and $0 < t_2^* < \frac{1}{\sqrt{q}+1}$. Also a semi-stable FP at $(t_1,t_2) = (-\frac{1}{q-1}, 0)$ is desirable $\forall q$; this situation is in fact encountered in the present RG only for $q = 2$ (we find, on the $t_2 = 0$ axis, a semi-stable FP located at $t_1 > \frac{1}{1-q}$ for $0 < q < 1$, at $t_1 < -\frac{1}{q-1}$ for $1 \leq q < 2$, at $t_1 > -\frac{1}{q-1}$ for $2 < q \leq q^*$; for $q \geq q^*$ this FP collapses with the (t_1^*, t_2^*) FP and leave the $t_2 = 0$ axis). This fact prevents, for $q \neq 2$, the $t_1 = -\frac{1}{q-1}$ axis from being self-renormalized as desirable (see Figs. 2.c and 2.d). In spite of these small inadequacies, the results, whenever can be checked, are numerically very satisfactory even for $b = 2$

as indicated in Fig. 3. Remark also that the q = 2 flux diagram (Fig. 2.b) is, as it should, completely symmetric with respect to the $t_1 = 0$ axis. The critical lines compare very well with that obtained by series expansion [4] (available only for q = 2), along the J_1, J_2 plane. For $J_1 = 2J_2$, for example, we obtained the value $J_1/k_B T_c = 0,25$ very close to the one presented in Ref. [4], namely 0,2628.

Let us finally recall that the Jacobian matrix

$$M \equiv \begin{pmatrix} \frac{\partial t_1'}{\partial t_1} & \frac{\partial t_1'}{\partial t_2} \\ \frac{\partial t_2'}{\partial t_1} & \frac{\partial t_2'}{\partial t_2} \end{pmatrix} \qquad (4)$$

calculated in the $(\frac{1}{\sqrt{q}+1}, 0)$, $(0, \frac{1}{\sqrt{q}+1})$ and (t_1^*, t_2^*) FP provides useful information concerning limiting slopes and critical exponents. These quantities will be discussed in Sections III and IV.

III - PARA-FERRO PHASE TRANSITION

In order to clarify the discussion of the results we have obtained concerning the para-ferro critical line, we shall present them in the following order: the $J_1 = 0$ case, the $J_2 = 0$ one and finally the $J_1 = J_2$ one.

III.1 - The $J_1 = 0$ case

In the fixed point $(t_1, t_2) = (0, \frac{1}{\sqrt{q}+1})$ (exact critical point) the Jacobian matrix M (Eq. (4)) is diagonal with both eigenvalues $\lambda_1 \equiv (\partial t_1'/\partial t_1)$ and $\lambda_2 \equiv (\partial t_2'/\partial t_2)$ larger than unity (furthermore $\lambda_1 > \lambda_2$, $\forall q$); the corresponding eigenvectors are

(1,0) and (0,1). The correlation length critical exponent is given by $\nu \equiv 1/y_T = \ell n b/\ell n \lambda_2$; the RG results herein obtained (Fig. 4a and Table I) are precisely those of Ref. [7] where t_1 was assumed vanishing from the very beginning of the problem (remark that, in the limit $t_1 \to 0$, the graph of Fig. 1.c coincides with that presented in Fig. 1.a of Ref. [7]; this property is in fact valid for all values of b). The crossover exponent ϕ (defined by $\frac{1}{\sqrt{q}+1} - t_2 \propto t_1^{1/\phi}$) is given by $\phi = \ell n \lambda_1 / \ell n \lambda_2$; by following along the lines of the argument presented in Appendix of Ref. [5] (which holds for any value of q if we take into account the cluster image[11] of the Potts model), one can easily prove that $\phi = \gamma$ where γ is the standard susceptibility critical exponent (we recall that $d_f \equiv 2 - \eta = 2(y_H - 1) = \gamma/\nu = \ell n \lambda_1 / \ell n b$ where η is the standard correlation function critical exponent); the RG results herein obtained (Fig. 4b and Table I) recover, for q = 1, those of Ref. [5].

Let us mention a technical point: the b = 3 and b = 4 d_f calculations were not performed through the complete knowledge of the recursive relations (3) but through that of the $t_1 \to 0$ leading terms. For example, for b = 3 we obtain, at the point $(t_1, t_2) = (0, \frac{1}{\sqrt{q}+1})$, that

$$\lambda_1 = 6t_A + 4t_B + 4t_A t_C + 2t_A t_D + 2t_B t_C + 2t_B t_D + 2t_C^2 + 2t_C t_D + t_D^2 \qquad (5)$$

where t_A, t_B, t_C and t_D are the transmissivities of the graphs indicated in Fig. 5.

III.2 - The $J_2 = 0$ case

In the fixed point $(t_1, t_2) = (\frac{1}{\sqrt{q}+1}, 0)$ (exact critical point) the Jacobian matrix M (Eq. (4)) is given by

$$M = \begin{pmatrix} \lambda_1 & \lambda_{12} \\ 0 & \lambda_2 \end{pmatrix} \qquad (6)$$

The eigenvalues are $\lambda_1 (\lambda_1 > 1, \forall q)$ and λ_2 (for $b = 2$, $\lambda_2 < 1$ if $q \gtrsim 1$ and $\lambda_2 > 1$ if $q \lesssim 1$); the corresponding eigenvectors are $(1,0)$ and $(-\lambda_{12}, \lambda_1 - \lambda_2)$ and the limiting slope of the critical line is $dt_2/dt_1 = (\lambda_2 - \lambda_1)/\lambda_{12}$ (for $b = 2$, $-dt_2/dt_1$ equals 0.753, 0.640, 0.561 and 0.505 for $q = 1, 2, 3$, and 4 respectively). The exponent ν is given by $\nu = \ell n b / \ell n \lambda_1$ and the RG results we obtain (see Fig.4.a and Table I) are precisely those of Ref. [12] (for example, in the limit $t_2 \to 0$, the graph of Fig. 1.d coincides with that of Fig. 1.c of Ref. [12]).

III.3 - The $J_1 = J_2$ case

Although the exact critical point corresponding to the $J_1 = J_2$ case is still unknown, good estimates are available[13] for $q \geq 1$: the comparison is performed in Table II. Remark that the RG results improve for increasing q: this is easy to understand if we take into account that for a given b-sized cell the RG error comes from the periphery of the cell,

and should therefore decrease for increasing b^q (b^q is proportional, in the limit $b \to \infty$, to the ratio of the number of bulk configurations to the number of peripheric ones).

Let us finally mention that, because of the exclusion of certain peripheric bonds (see caption of Fig. 1 and Refs. [5,6]), an error is introduced into our RG. As a consequence of this error a spurious semi-stable FP appears, for sufficiently small q ($q \lesssim 1$) in the vicinity of the $(\frac{1}{\sqrt{q}+1}, 0)$ FP (for example, for $b = 2$ and $q = 1$, its location is (0.486, 0.010); see Fig. 2.a); the inexistence of this spurious FP for larger values of q ($q \gtrsim 1$) comes oncemore from the improvement associated with the $b^q \to \infty$ limit.

IV - PARA-ANTIFERRO PHASE TRANSITION

The para-antiferro critical line is clearly controlled by the $(0, \frac{1}{\sqrt{q}+1})$ and (t_1^*, t_2^*) FP. In what concerns the former, the associated Jacobian matrix has already been discussed in Section III.1. In particular the para-antiferro critical line is, as the para-ferro one and for the same reason, tangencial to the $t_1 = 0$ axis for all q. Furthermore both y_T and y_H critical exponents are the same; we believe this holds for the complete $J_2 \geq 0$ critical region.

The location of the (t_1^*, t_2^*) FP has been discussed in Section II (see also Fig. 3). The associated Jacobian matrix M (Eq. (4)) has the same form presented in Eq. (6) with $\lambda_1 > 1$ and $\lambda_2 < 1$ for $q < q^*$. The limiting $t_2 \to 0$ slope of the critical line is $dt_2/dt_1 = 0.752$ for $q = 1$; we recall that, for $q = 2$, the

para-ferro and para-antiferro critical lines are symmetric. For $q > q^*$ the vector (1,0) is no longer an eigenvector, which is a desirable fact from the physical standpoint (see discussion in Section II); unfortunately, the other eigenvector is not (0,1) (this is related to the fact that the (t_1^*, t_2^*) FP is not located at the $t_1 = -\frac{1}{q-1}$ axis) as physically expected. Because of this reason the values for ν associated with the (t_1^*, t_2^*) FP are not numerically satisfactory.

V - NEGATIVE VALUES FOR J_2

If we allow J_2 to take both negative and positive values, the $q = 2$ phase diagram is known [3] to be of the type schematically indicated in Fig. 6.a: four phases are possible, namely the para-(P), ferro-(F), antiferro-(AF) and super antiferromagnetic (SAF) ones (see Fig. 6). The q-evolution of this phase diagram is, to the best of our knowledge, still unknown; in particular it is not excluded that, for $q > 2$, the phase diagram becomes even richer than indicated in Fig. 6.a. The study of this problem should be very interesting; unfortunately computer limitations prevented us from performing it. The purpose of this section is to present the RG cells we propose for this study. These cells are indicated in Fig. 7, and they should be convenient in spite of the fact that, in the $J_2 < 0$ region, frustration is present. One of the RG recursive relations is obtained by using the A "entrances" and the B "exits" of the cells; the other one is obtained by replacing the B "exits" by the C ones.

In order to understand the process which provided the cells indicated in Fig. 7, let us first analyze the T = 0 configurations presented in Fig. 6. We remark that the α-sublattice (see Fig. 6.b) of the AF configuration (Fig. 6.d) precisely reproduces the F configuration (Fig. 6.c) of the whole lattice. Furthermore the α-sublattice of the SAF configuration (Fig. 6.e) precisely reproduces the AF configuration (Fig. 6.d) of the whole lattice. We use these topological properties for constructing the RG cells of Fig. 7. The b = 2 cell used in the previous sections (see Fig. 1.c) was constructed by superimposing two ⊞-shaped cells (very convenient[7] for the simple square lattice, as they provide the exact critical point for all q), one for each sublattice (α and β), and connecting them through new first-neighbor bonds. Analogously the cell of Fig. 7.b was constructed by superimposing two cells of the kind presented in Fig. 1.c (where only the dashed bonds were retained), one for each sublattice, and connecting them by new first-neighbor bonds (now dashed in Fig. 7.b)

VI - CONCLUSION

We have discussed, within a real space renormalization group framework, the q-state Potts model in first- and second-neighbor square lattice by allowing both signs for the first-neighbor coupling constant J_1, but only positive sign for the second-neighbor J_2 one. The q-evolution of the full phase diagram was obtained and the results are both qualitatively and

quantitatively satisfactory; in particular the exact result is obtained for $J_1 = 0$ as well as for $J_2 = 0$ and $J_1 > 0$; for $J_2 = 0$ and $J_1 < 0$ the result is quite close to the exact one (for $q = 0$ and $q = 2$ is precisely the exact one). Also the $J_1 = J_2$ results compare well with previous ones.

The $J_1 \to 0$ crossover behavior (corresponding to the decoupling of the lattice into two independent simple square sublattices) enables us to calculate, besides the thermal critical exponent y_T, the magnetic critical one y_H without introducing any external magnetic field (neither ghost sites). The q-dependence of both y_T and y_H compare well with the possibly exact available proposals.

Finally we propose a new kind of renormalization group cells which presumably are quite convenient for including into the present discussion the $J_2 < 0$ region, where a new phase (namely the superantiferromagnetic one) hopefully exists.

One of us (C.T.) aknowledges a Fellowship from the Guggenheim Foundation.

REFERENCES

[1] M.P.M den Nijs, J. Phys. A 12, 1857 (1979)

[2] B. Nienhuis, E.K. Riedel and M. Schick, J. Phys. A 13, L 189 (1980)

[3] J.M.J. Van Leeuwen, Phys. Rev. Lett. 34, 1056 (1975)

[4] J. Oitmaa, J. Phys. A 14, 1159 (1981)

[5] R. Riera, P.M. Oliveira, C.M. Chaves and S.L.A. de Queiroz, Phys. Rev. B 22, 3481 (1980)

[6] P.M. Oliveira, Phys. Rev. Lett. 47, 1423 (1981)

[7] C. Tsallis and S.V.F. Levy, Phys. Rev. Lett. 47, 950 (1981)

[8] N. Jan and L.L. Mosely, Can. J. Phys. 57, 1800 (1979)

[9] R.B. Potts, Proc. Camb. Phys. Soc. 48, 106 (1952)

[10] R.J. Baxter, to be published (Proc. Roy. Soc. London)

[11] P.W. Kasteleyn and C.M. Fortuin, J. Phys. Soc. Japan, Suppl. 26, 11 (1969)

[12] P.M. Oliveira, and C. Tsallis, J. Phys. A 15, 2865 (1982)

[13] C. Tsallis and A.C.N. de Magalhães, J. Physique/Lettres 42, L 227 (1981)

TABLE CAPTIONS

Table I - Values of the critical exponents d_f(at $(t_1,t_2) = (0, \frac{1}{\sqrt{q}+1})$) and ν ((a) at $(t_1,t_2) = (0, \frac{1}{\sqrt{q}+1})$; (b) at $(\frac{1}{\sqrt{q}+1}, 0)$) The values b =3/2 (b = 4/3) correspond to renormalizing the b = 3 (b = 4) cell into the b = 2 (b = 3) one.

Table II - Values of the b = 2 critical transmissivities for the $J_1 = J_2$ case, compared with conjectural estimates [13].

TABLE I

			q = 1	q = 2	q = 3	q = 4
b = 2	d_f		2.299	2.063	1.907	1.788
	ν	a	1.428	1.149	1.024	0.948
		b	1.042	0.864	0.785	0.738
b = 3	d_f		2.180	1.955	1.807	1.693
	ν	a	1.380	1.109	0.988	0.916
		b	1.099	0.899	0.811	0.758
b = 4	d_f		2.121	1.919	1.779	1.668
	ν	a	1.363	1.095	0.975	0.903
b = 3/2	d_f		1.976	1.769	1.635	1.530
	ν	a	1.305	1.048	0.933	0.865
		b	1.212	0.967	0.859	0.794
b = 4/3	d_f		1.896	1.781	1.672	1.576
	ν	a	1.302	1.043	0.928	0.859
exact [1,2] (conjectural)	d_f		1.791...	1.75	1.733...	1.75
	ν		1.333...	1	0.833...	0.666...

TABLE II

	q = 1	q = 2	q = 3	q = 4
RG (b = 2)	0.210	0.171	0.148	0.133
conjectural[13]	0.249 ± 0.011	0.188 ± 0.006	0.157 ± 0.006	0.137 ± 0.006

FIGURE CAPTIONS

Fig. 1 - Cells (and corresponding graphs) used for the RG calculations. The arrows indicate the entrances and exits. α and β represent the sublattices decoupled in the limit of vanishing first-neighbor interaction. In the graphs, full (open) circles correspond to internal (terminal) points. (a) Renormalized second-neighbor transmissivity t_2'; (b) renormalized first-neighbor transmissivity t_1'; (c) original second-neighbor transmissivity t_2; (d) original first-neighbor transmissivity t_1. In (a) and (c), the upper dashed bonds are excluded from the corresponding graphs in order to preserve the symmetry between the α and β sublattices [5,6]

Fig. 2 - Flux diagrams for $b = 2$. (a) $q = 1$, $(t_1^*, t_2^*) = (-0.325, 0)$; (b) $q = 2$, $(t_1^*, t_2^*) = (1-\sqrt{2}, 0)$; (c) $q = 3$, $(t_1^*, t_2^*) = (-0.375, 0.150)$; (d) $q = 4$, $(t_1^*, t_2^*) = (-0.260, 0.221)$. The open circle is the fully unstable FP, the full circles are the semi-stable FP, and the squares are stable FP. The arrows indicate the local flow direction. P, F and AF represents the para-, ferro-and antiferromagnetic phases, respectively.

Fig. 3 - q-evolution of the phase diagram for the simple square lattice ($t_2 = 0$). The dashed line represents the exact result [10], and the full line corresponds to the present RG calculation for $b = 2$. The exact and RG (for all b) curves coincide for $J_1 > 0$ and also for $J_1 < 0$ at

the points $q \to 0$ and $q = 2$. The $J_1 \to -\infty$ asymptotic values of q^* are indicated for $b = 2$ and $b = 3$.

Fig. 4 - q-evolution of the critical exponents $\nu \equiv 1/y_T$ (a) and $d_f \equiv 2(y_H - 1)$ (b). Dashed lines correspond to the conjectures of den Nijs [1] for y_T and of Nienhuis et al [2] for y_H. In part (a) the curves 1 and 2 are obtained at the points $(t_1, t_2) = (0, \frac{1}{\sqrt{q}+1})$ for $b = 4$, and $(\frac{1}{\sqrt{q}+1}, 0)$ for $b = 3$ respectively.

Fig. 5 - Cells and graphs used for calculating λ_1 (Eq. (5)) in the $b = 3$ case.

Fig. 6 - (a) Schematic phase diagram for the first-and second-neighbor square lattice Ising model ($q = 2$); (b) Sublattices α and β in which the whole lattice is decoupled in the $J_1 = 0$ limit; (c) $T = 0$ configuration of the ferromagnetic (F) Ising phase; (d) $T = 0$ configuration of the antiferromagnetic (AF) Ising phase; (e) $T = 0$ configuration of the super antiferromagnetic (SAF) Ising phase.

Fig. 7 - Proposed RG cells for the study of the whole phase diagram (including $J_2 < 0$) of the first-and second-neighbor square lattice q-state Potts model. (a) Renormalized cell; (b) original cell.

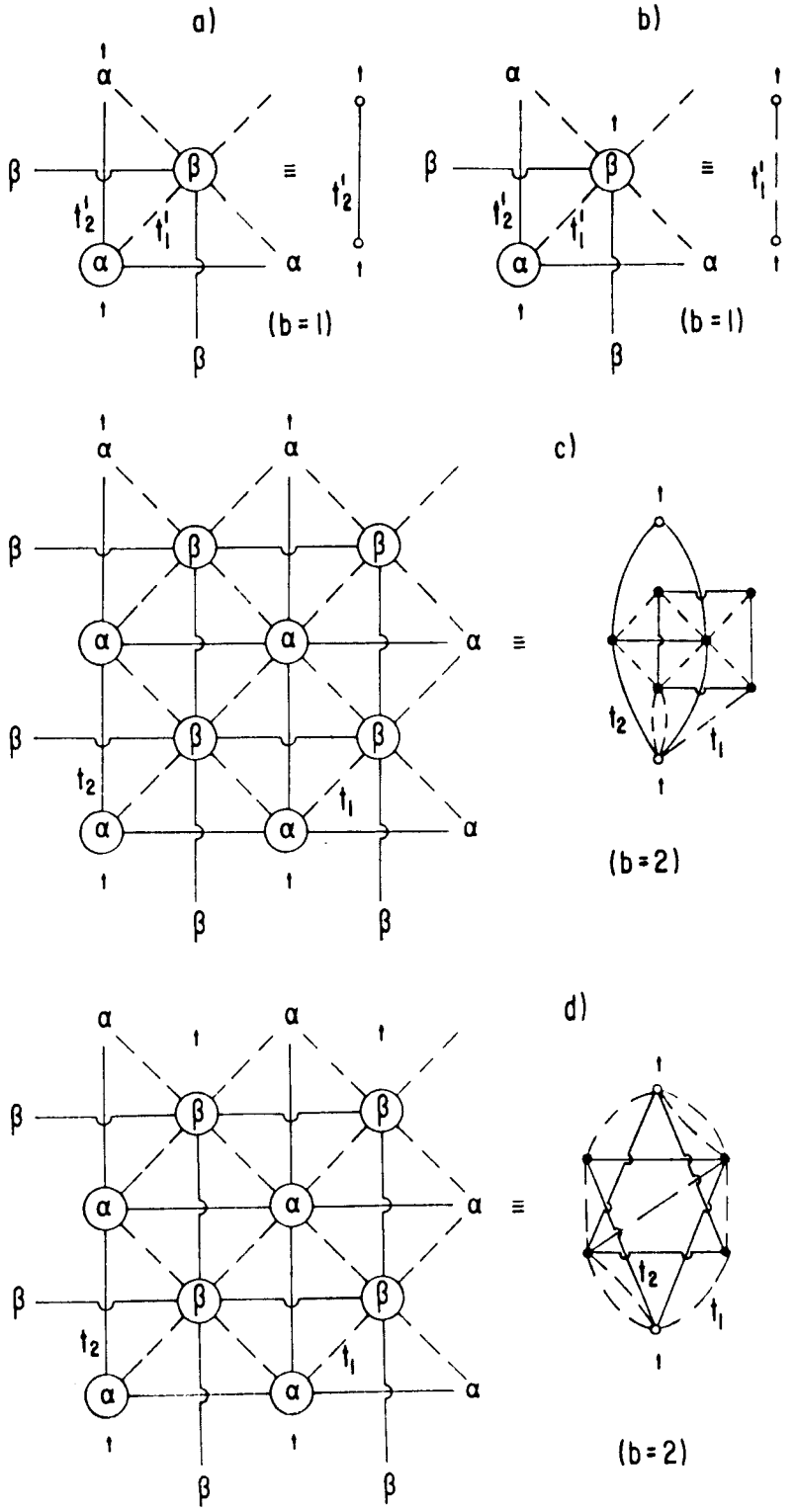

FIG.1

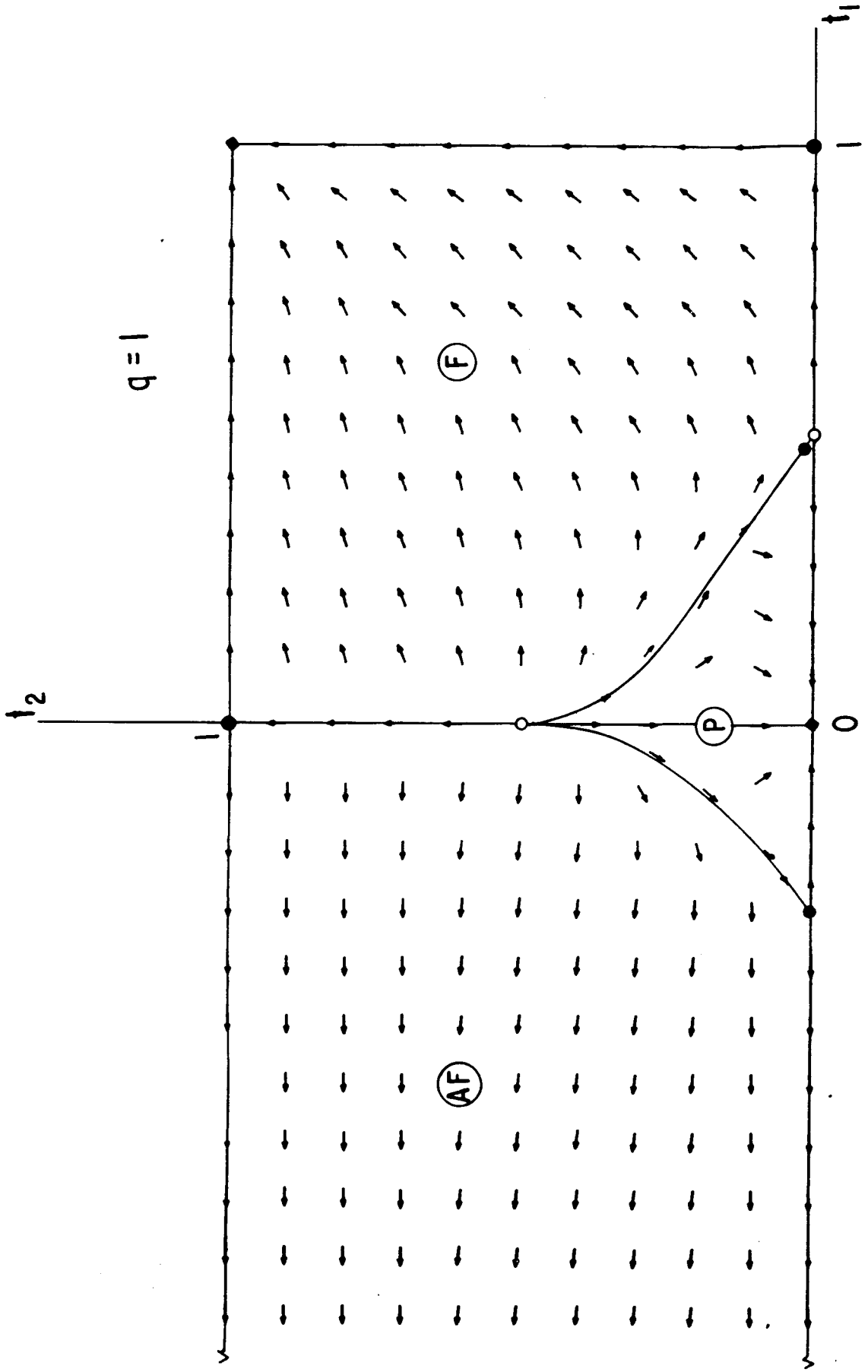

FIG.2a

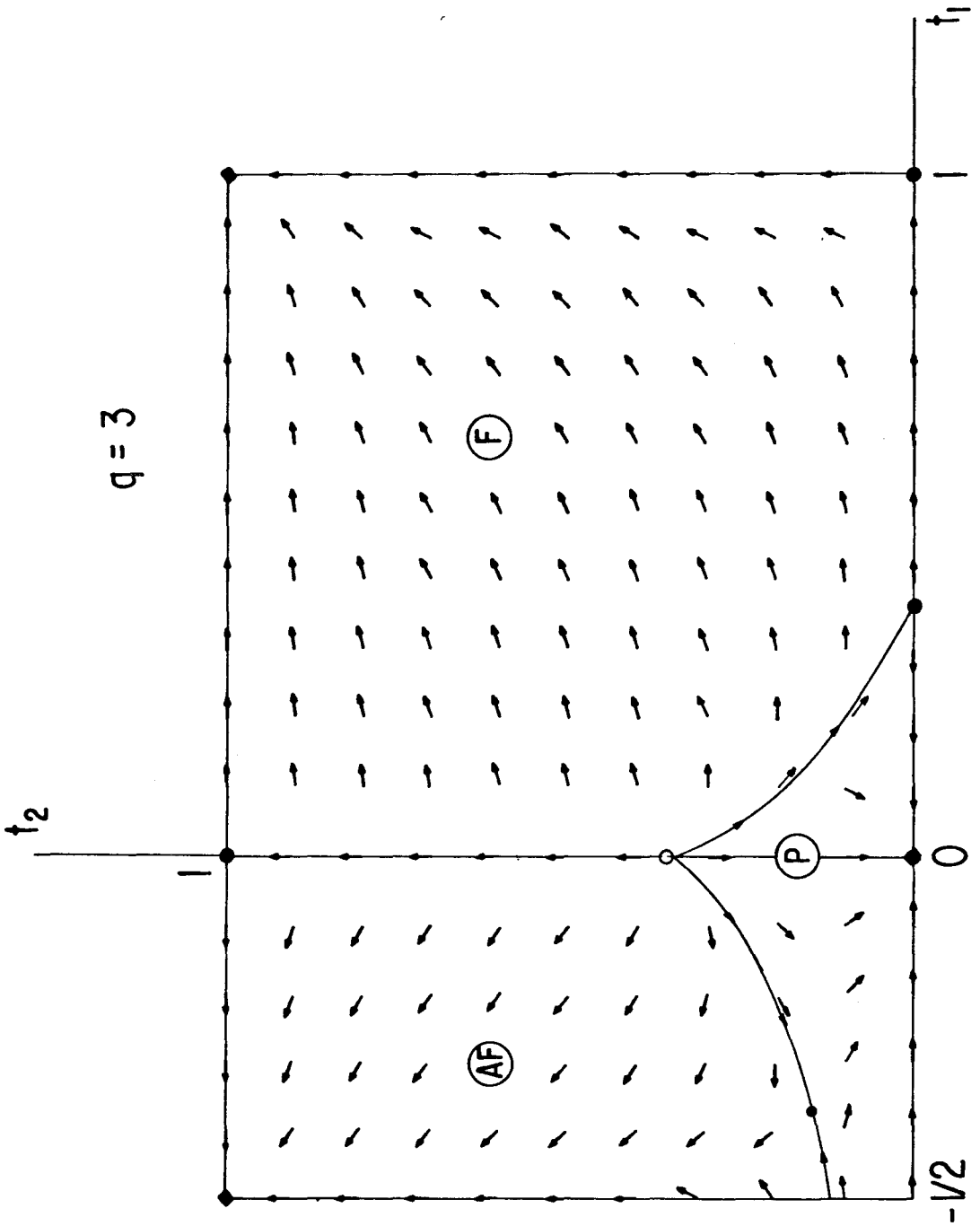

FIG.2c

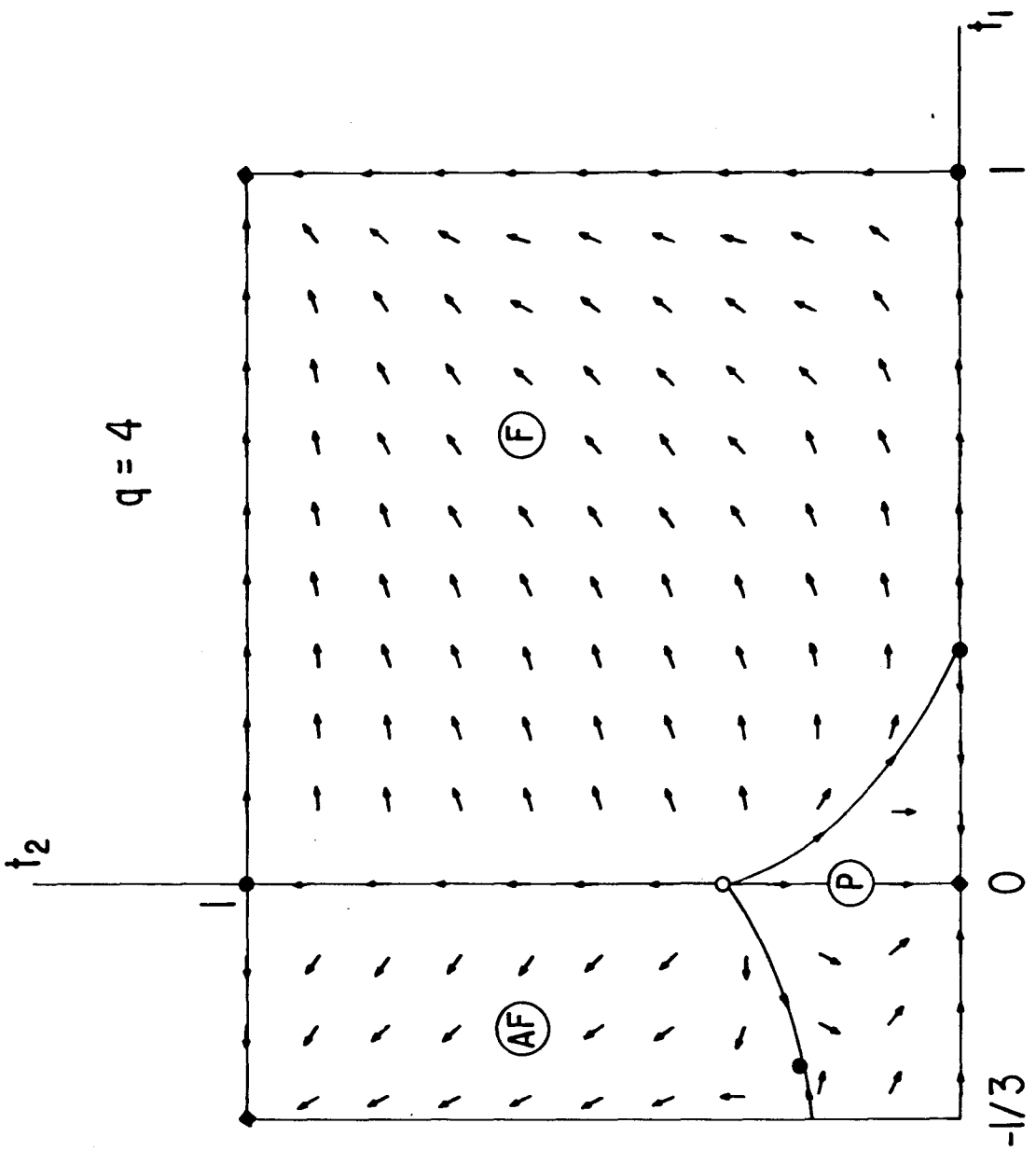

FIG.2d

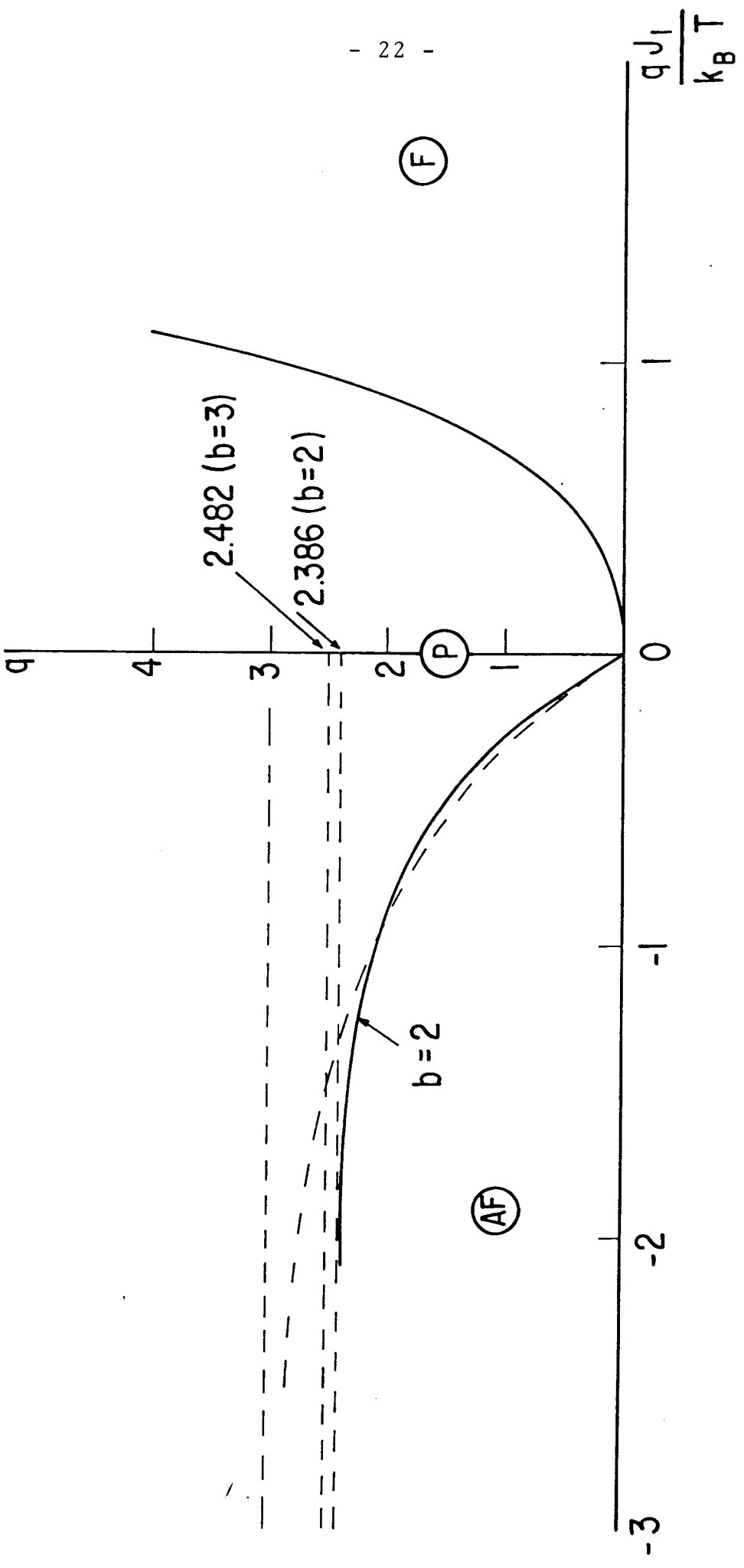

FIG. 3

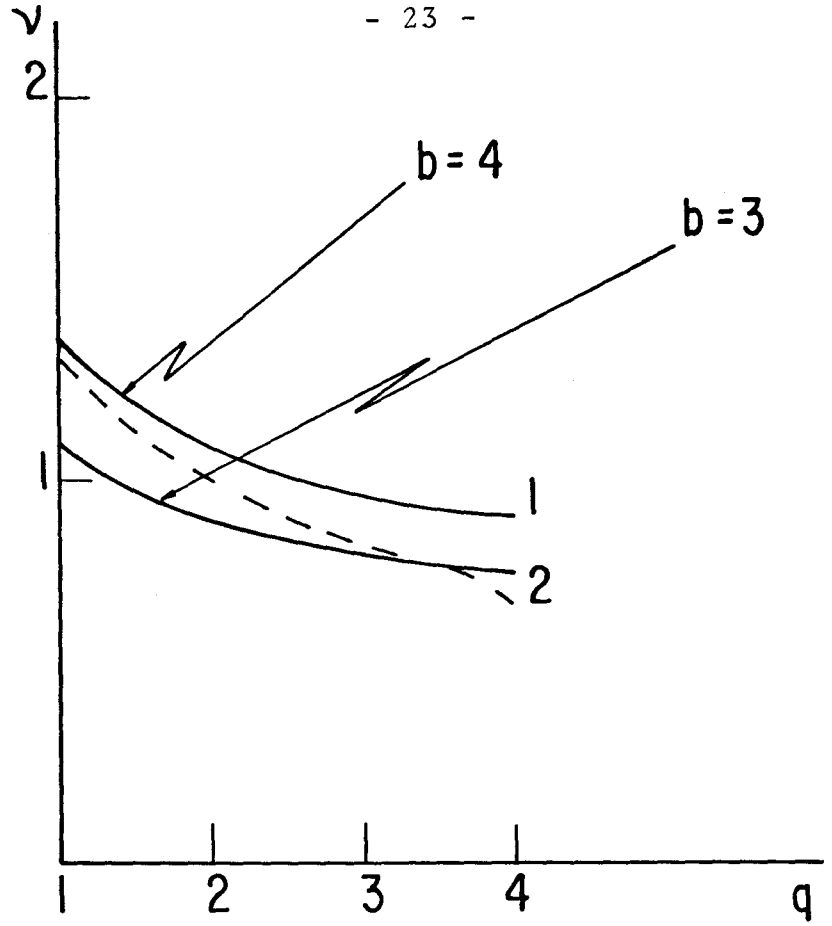

a)

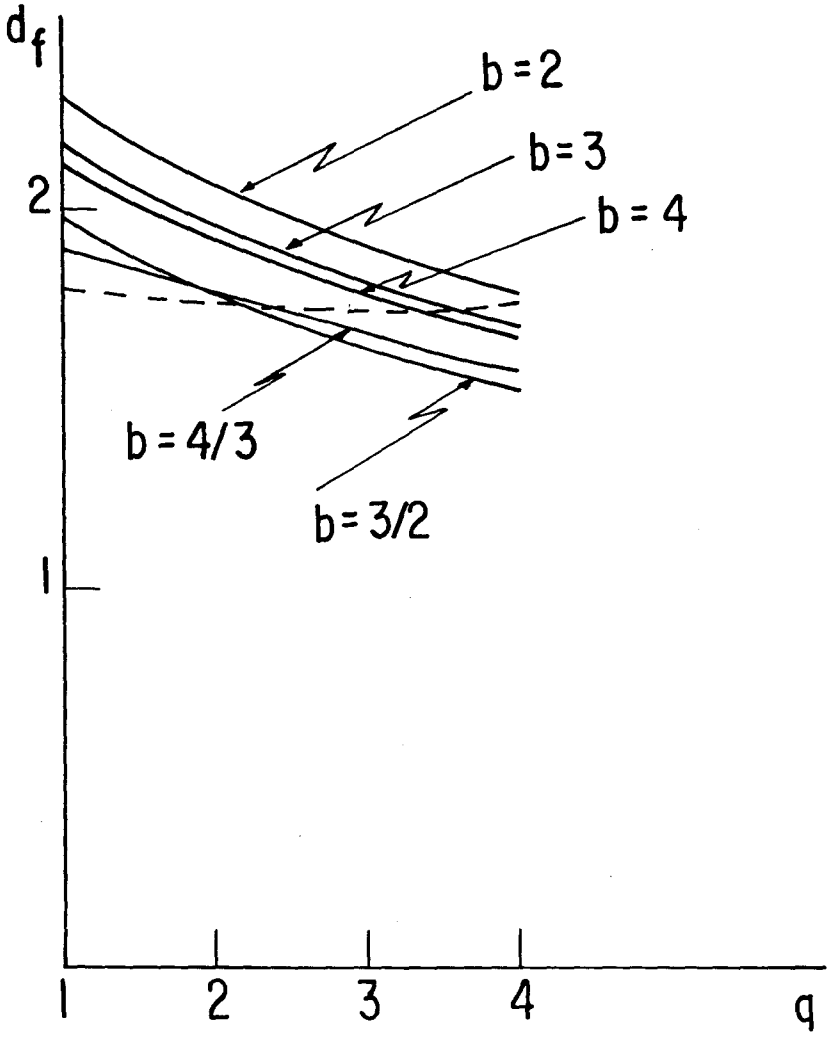

b)

FIG. 4

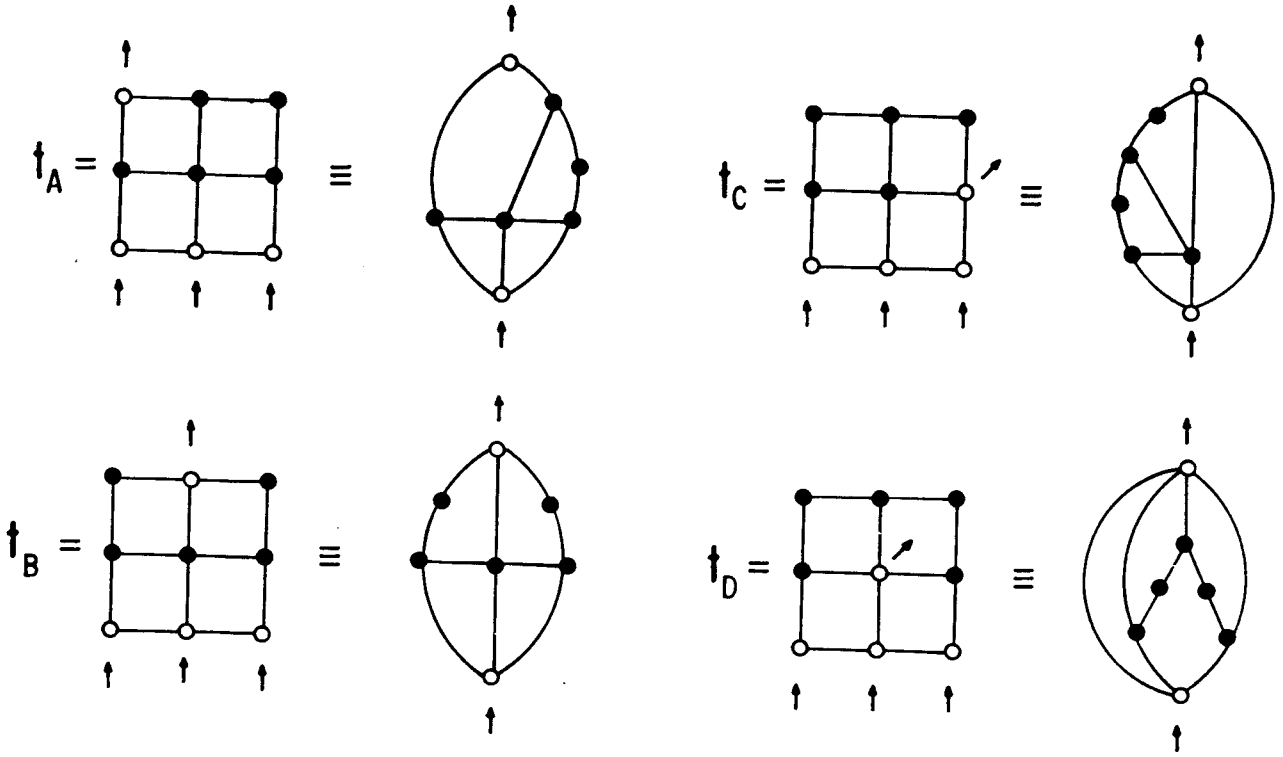

FIG.5

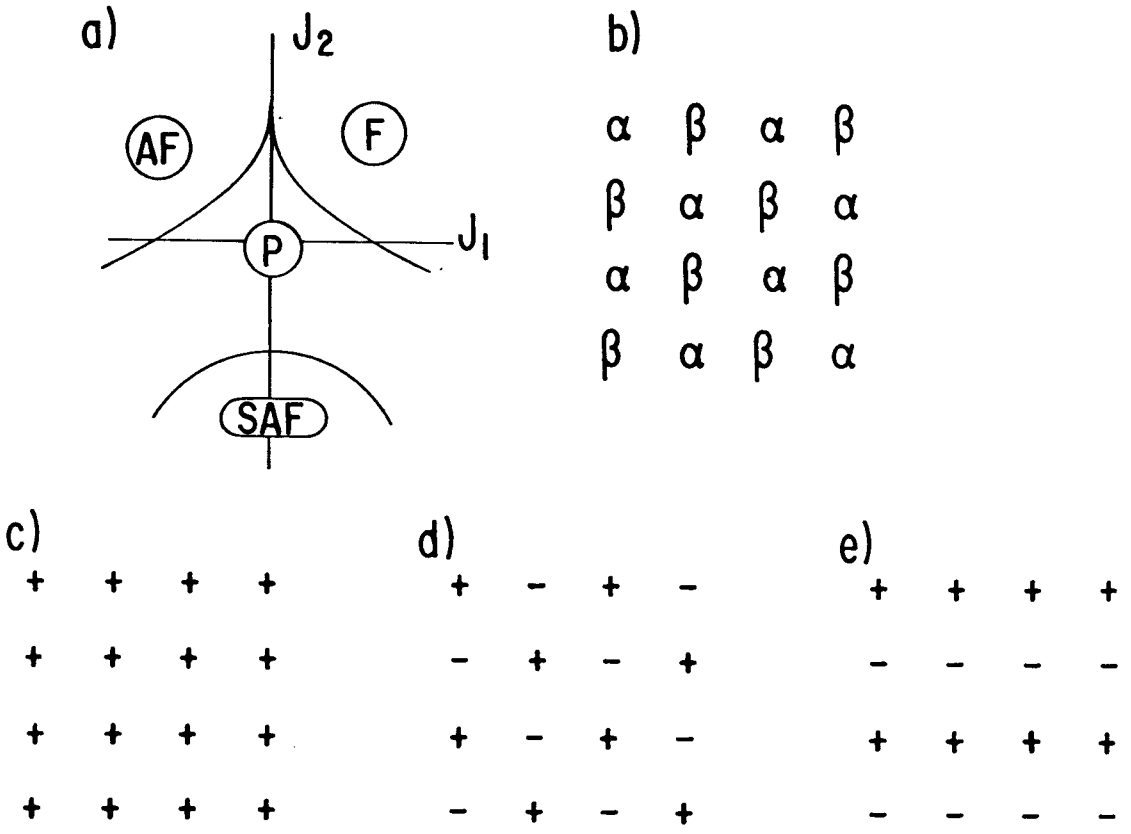

FIG. 6

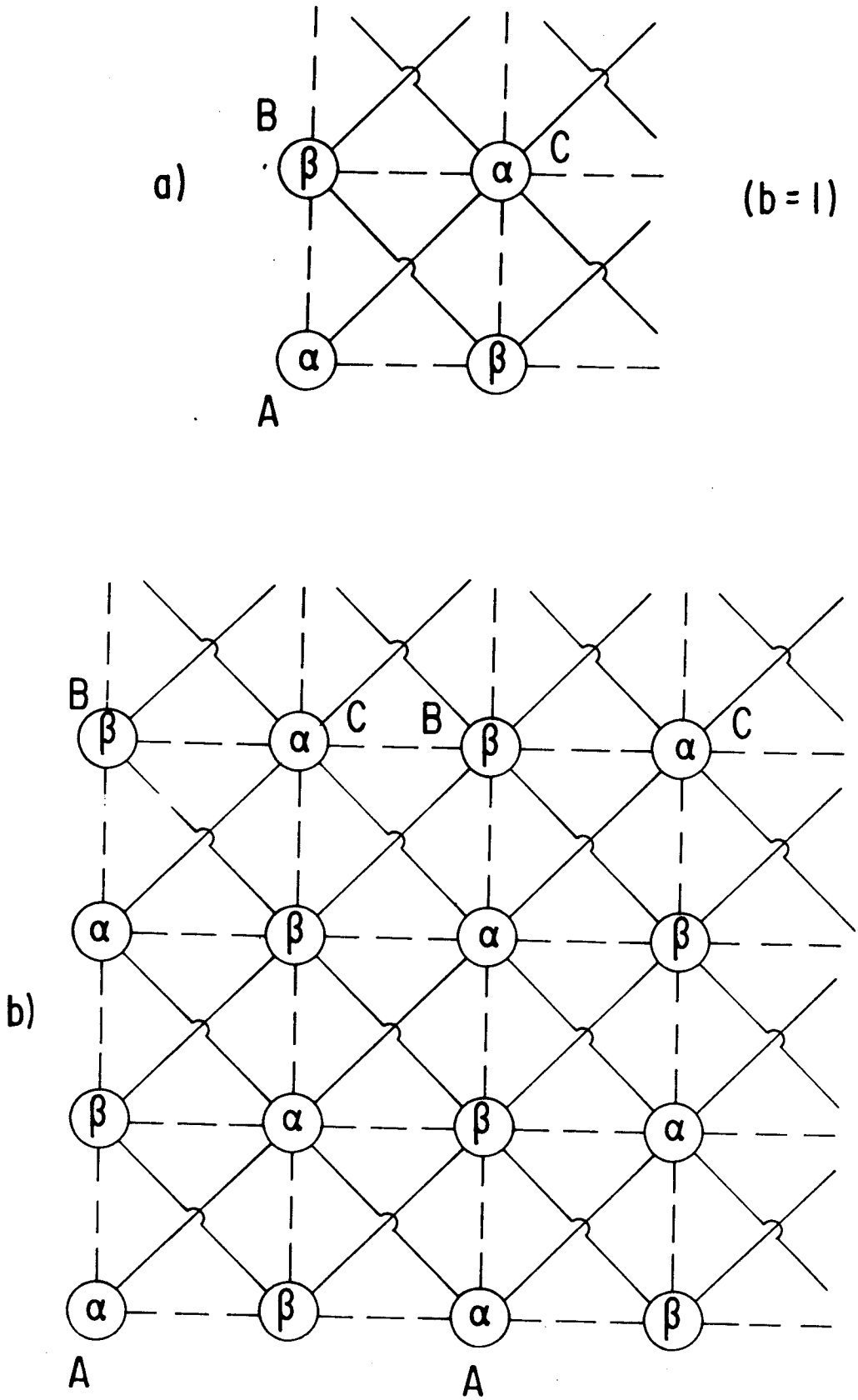

FIG. 7